THE ASTROPHYSICAL JOURNAL, 489:656–671, 1997 November 10

THE ULTRAVIOLET PROPERTIES OF THE NARROW-LINE QUASAR I Zw 1

ARI LAOR
Physics Department, Technion, Haifa 32000, Israel; laor@physics.technion.ac.il
AND
BUELL T. JANNUZI, RICHARD F. GREEN, AND TODD A. BOROSON
National Optical Astronomy Observatories, P.O. Box 26732, 950 North Cherry, Tucson, AZ 85726-6732
Received 1997 March 13; accepted 1997 June 24

ABSTRACT

I Zwicky 1 (I Zw 1) is the prototype narrow-line quasar. Its narrow-line profiles minimize blending effects and thus allow a significantly more accurate study of individual quasar emission lines. We report here the results of our study of the 1150–3250 Å emission of I Zw 1 using a high signal-to-noise (50–120) spectrum obtained with the Faint Object Spectrograph of the *Hubble Space Telescope*. The UV spectrum of I Zw 1 is very rich in emission lines, with essentially no wavelength range free of emission-line features. The following main new results are obtained:

1. The Mg II λ2798 doublet is partially resolved, and the measured doublet ratio is 1.2/1. This ratio verifies theoretical predictions that the Mg II λ2798 line is thermalized in the broad-line region (BLR).
2. The Al III λ1857 doublet is clearly resolved, with a thermalized doublet ratio of 1.25/1. The line optical depth provides an upper limit to the clouds' distance from the ionizing source that is consistent with the "standard" BLR radius.
3. A weak associated UV absorption system is detected in N V (possibly also in C IV and Lyα as well), suggesting an outflow with a velocity of $\sim$1870 km s^{-1} and velocity dispersion of $\lesssim$300 km s^{-1}.
4. Lines from ions of increasing ionization level show increasing excess blue-wing flux and an increasing line peak velocity shift, reaching a maximum blueshift of $\sim$2000 km s^{-1} for He II λ1640. This may indicate an outflowing component in the BLR, where the ionization level increases with velocity and which is visible only in the approaching direction. The highest velocity part of this outflow may produce the associated UV absorption system.
5. The small C III] λ1909 equivalent width and the small C III] λ1909/Lyα and C III] λ1909/Si III] λ1892 flux ratios indicate a typical BLR density of $n_e \sim 10^{11}$ cm^{-3}, i.e., about an order of magnitude larger than that implied by C III] λ1909 in most quasars. A BLR component with a density $n_e \gtrsim 10^{11}$ cm^{-3} is implied by the EW and doublet ratio of the Al III λ1857 doublet.
6. Prominent Fe II UV 191 emission is seen, together with weaker line emission at 1294 Å and 1871 Å. These three features have been proposed by Johansson & Jordan as evidence for significant Lyα pumping of the 8–10 eV levels of Fe II.
7. Significant Fe III emission is present. The Fe III UV 34 and UV 48 multiplets are clearly resolved, and Fe III UV 1, UV 47, UV 50, and UV 68 may also be present. The implications of significant Fe III emission for the conditions in the BLR need to be explored.
8. Very weak [C III] λ1907 and [Si III] λ1883 emission may be present, suggesting a narrow-line-region component with $n_e \sim 5 \times 10^5$ cm^{-3}.

The rich UV emission spectrum of I Zw 1 should serve as a useful "template" for the identification of weak features in other active galactic nuclei and as a useful benchmark for photoionization models, in particular, for models of the complex Fe II emission spectrum.

Subject headings: quasars: absorption lines — quasars: emission lines — quasars: individual (I Zwicky 1) — ultraviolet: galaxies

1. INTRODUCTION

The prominent broad emission lines of quasars are typically blended with weaker emission features, such as emission from various Fe II multiplets. This blending prevents a reliable study of the prominent line profiles, the measurement of weaker lines, and the identification of very weak lines. Even in high signal-to-noise (S/N) spectra (e.g., Laor et al. 1994a), the blending of features prevents a reliable study of the individual line profiles of even the most prominent lines. Blending effects are minimized in the rare class of narrow-line quasars (i.e., with FWHM $\lesssim$1000 km s^{-1}). Therefore, the study of such objects can lead to a significantly more accurate study of the properties of individual emission lines.

I Zwicky 1 (I Zw 1) is the prototype narrow-line Seyfert 1 galaxy (NLS1). Its optical spectrum reveals narrow emission lines and strong Fe II emission (Sargent 1968; Phillips 1976, 1978; Oke & Lauer 1979). The NLS1 class of active galactic nuclei (AGNs) also tends to have weak [O III] $\lambda\lambda$4959, 5007 emission, asymmetric Hβ profiles (Boroson & Green 1992, hereafter BG92), steep soft X-ray spectra (Laor et al. 1994b, 1997a; Boller, Brandt, & Fink 1996), and possibly strong IR emission (e.g., Lipari 1994). Although I Zw 1 is classified as a Seyfert 1 galaxy, its absolute luminosity,

$M_V = -23.8$ (for $H_0 = 50$ km s^{-1} Mpc^{-1}, $q_0 = 0$), actually qualifies it as a low-luminosity quasar (Véron-Cetty & Véron 1991); we therefore refer to it as a quasar throughout the paper.

In this paper we describe a detailed study of the UV emission-line spectrum of I Zw 1 obtained with the Faint Object Spectrograph (FOS) of the *Hubble Space Telescope* (*HST*). An earlier UV spectrum of I Zw 1 obtained with the *International Ultraviolet Explorer* (*IUE*) is described by Wills (1983), and *HST* UV spectropolarimetry of I Zw 1 is described by Smith et al. (1997). Our study has two main goals. The first goal is to provide a detailed "identification template" of the UV emission features present in the spectra of quasars. The second goal of this study is to provide a high S/N Fe II UV emission template. The strong and narrow Fe II emission lines in I Zw 1 make it an ideal object for the construction of such a template, as was clearly demonstrated in the optical regime by BG92. Such a template is also important for studies of UV Fe II emission in AGNs (e.g., Netzer & Wills 1983; Wills, Netzer, & Wills 1985; Collin-Souffrin & Dumont 1986). These studies are important for understanding the physics of the broad-line region (BLR) since Fe II is a major, and sometimes the dominant, coolant of the BLR (e.g., Phillips 1977, 1978; Miley & Miller 1979; Bergeron & Kunth 1984; Joly 1981; Lipari, Terlevich, & Macchetto 1993). The Fe II template is also important for studies of lines strongly blended with Fe II, such as Mg II λ2798.

In this paper we concentrate on the first goal of this project. In § 2 we describe the observations and present the "identification template." In § 3 we discuss various diagnostics provided by some of the UV lines, and in § 4 we describe the physical properties of an associated UV absorption system and discuss its possible relationship to observed UV emission and X-ray absorption. A brief discussion of the similarities of I Zw 1 to broad absorption line quasars (BALs) (§ 5) and a summary of our main conclusions (§ 6) complete the paper.

2. OBSERVATIONS AND ANALYSIS

We obtained high S/N spectra (50–120 per resolution element) of I Zw 1 with the three high-resolution ($R = 1300$) gratings of the FOS from 1150 to 3280 Å. This S/N is comparable to the highest S/N yet obtained with *HST* for bright AGNs. All the observations were made using the 0.″86 aperture. The dates of the observations are G130H, 1994 February 13 (UT); G190H and G270H, 1994 September 14. The *HST* spectra were reduced as described in Schneider et al. (1993). The wavelength zero points of the three *HST* spectra were set using Galactic interstellar medium (ISM) absorption lines (Savage et al. 1993). The size of the necessary shift and the lines used for each of the three spectra (G130H, G190H, and G270H) were, respectively, 0.36 Å (Si II λ1526.71), 1.08 Å (Al II λ1670.79), and 0.99 Å (Fe II lines). We also obtained a complimentary high-resolution ground-based spectrum that covers the range from 3183 to 4074 Å. The spectrum was obtained using the Kitt Peak National Observatory 2.1 m telescope and Goldcam spectrograph on 1995 September 22 UT. The grating used was a 837 lines mm^{-1} grating, used in the second order, providing a dispersion of approximately 0.47 Å per pixel and a spectral resolution of 1.2 Å. The Ca II $\lambda\lambda$3933.66, 3968.47 doublet absorption by the ISM was used to secure a zero-point wavelength that matches the UV zero points, which were also set using lines of low-ionization-state ions. The optical spectrum is used in order to get complete coverage of the 2000–4000 Å region, required for generating the Fe II template.

Figure 1 presents the overall optical-UV spectrum of I Zw 1 from 1100 to 6000 Å. The spectrum was corrected for the effects of Galactic extinction of $E(B-V) = 0.1$ using the standard Seaton (1979) reddening curve. The extinction is

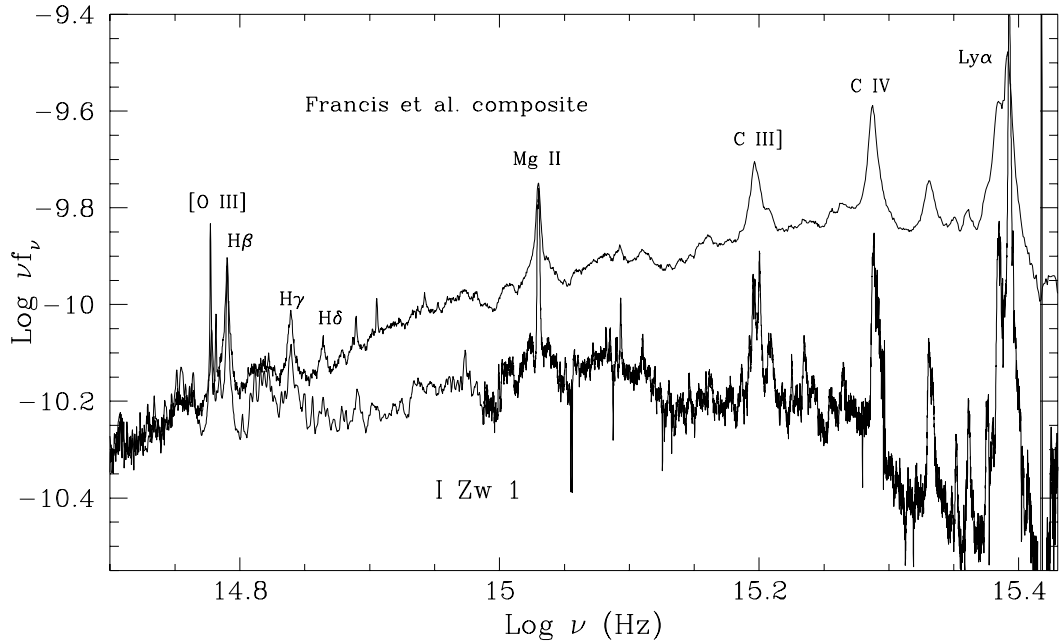

FIG. 1.—The optical-UV emission of I Zw 1, corrected for Galactic reddening [for $E(B-V) = 0.1$], vs. the Francis et al. composite (set to match I Zw 1 at log $\nu = 14.7$). Note that there is practically no wavelength range without significant emission features. Many of the very weak features in the Francis et al. composite are clearly resolved in the I Zw 1 spectrum. The optical spectrum of I Zw 1 was available through the courtesy of B. Wills.

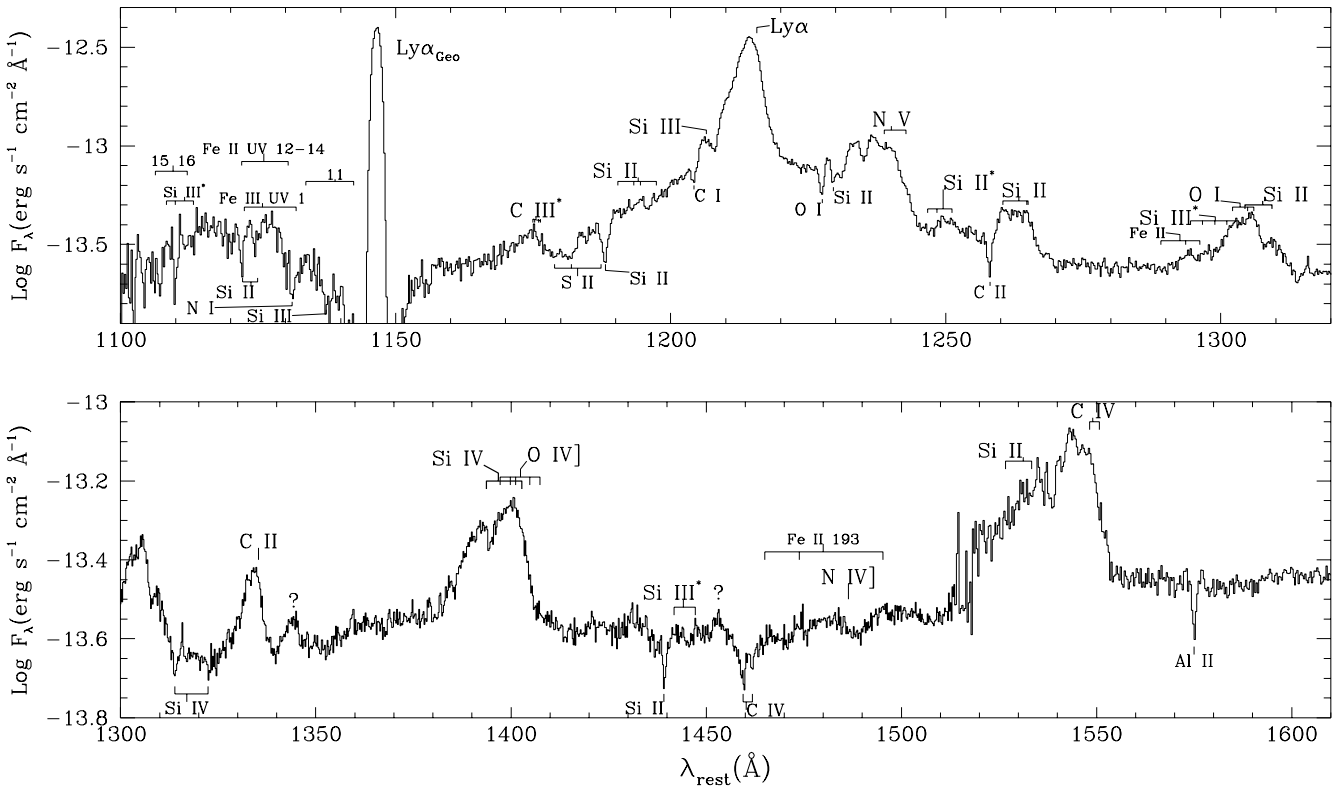

FIG. 2*a*

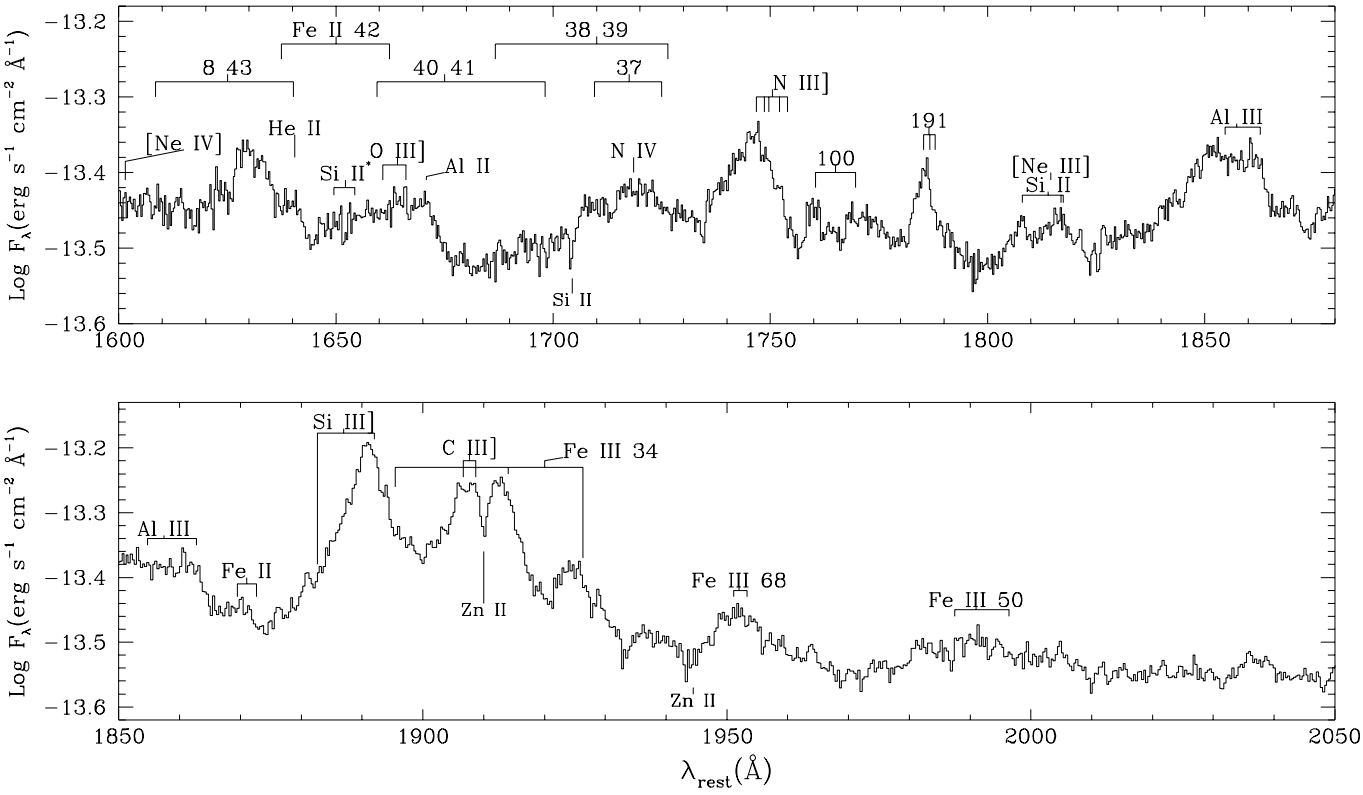

FIG. 2*b*

FIG. 2.—(*a*) Tentative identifications of most of the emission features in the *HST* FOS spectrum of I Zw 1. The lines indicate the expected wavelength for $z = 0.0608$. Only a small number of the Fe II multiplets that may be present were marked. Line designations below the spectrum refer to Galactic absorption features. (*b*) Same as (*a*). (*c*) Same as (*a*). (*d*) The optical spectrum. Note that the absolute flux calibration is not secure. The overlapping *HST* spectrum is plotted as a dotted line at $\lambda < 3100$ Å. This spectrum was shifted down by 0.37 in log flux to match the optical spectrum.

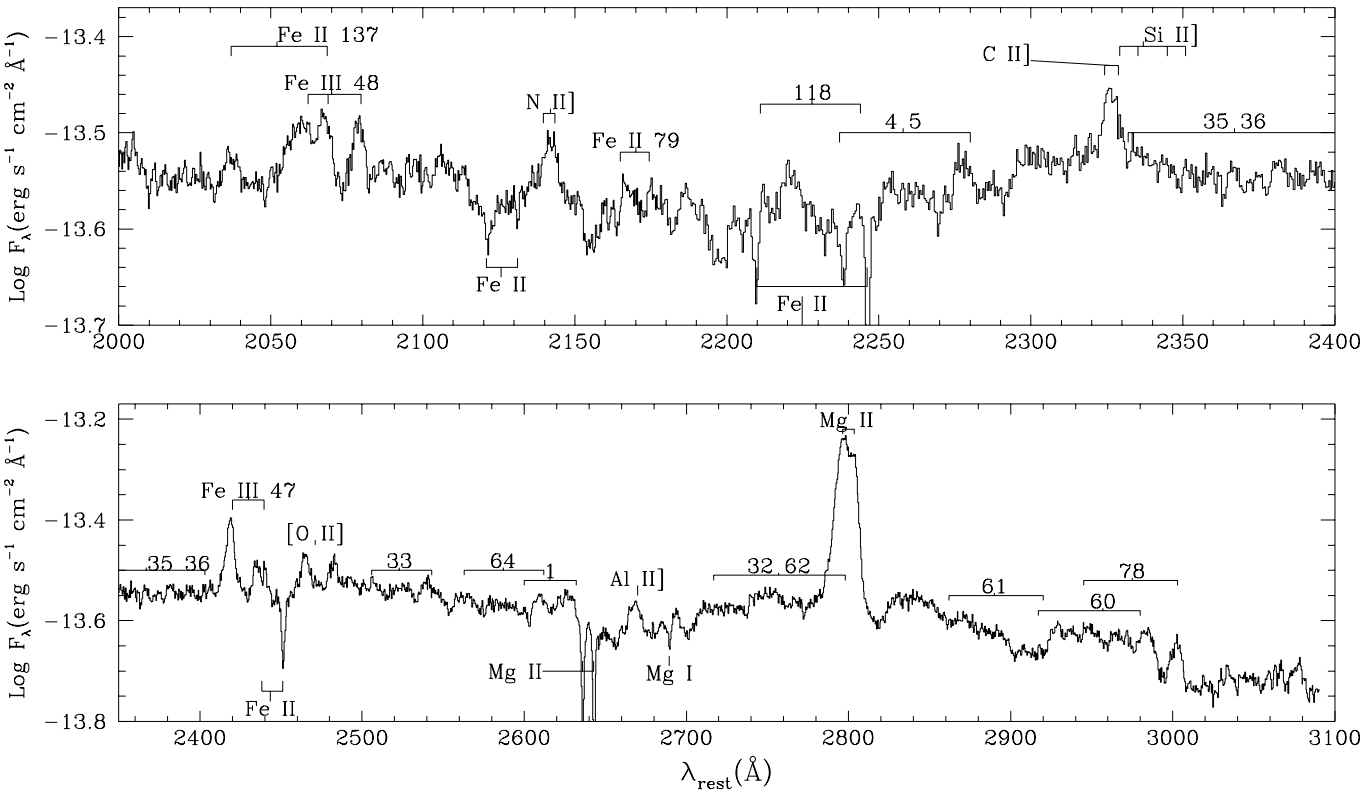
Fe II 137
Fe III 48
N II]
Fe II 79
118
4,5
C II]
Si II]
35,36
Fe II
Fe II
Log F$_\lambda$(erg s^{-1} cm^{-2} Å^{-1})
Fe III 47
[O II]
35,36
33
64
1
Al II]
32,62
Mg II
61
60
78
Mg II
Mg I
Fe II
λ_{rest}(Å)

FIG. 2*c*

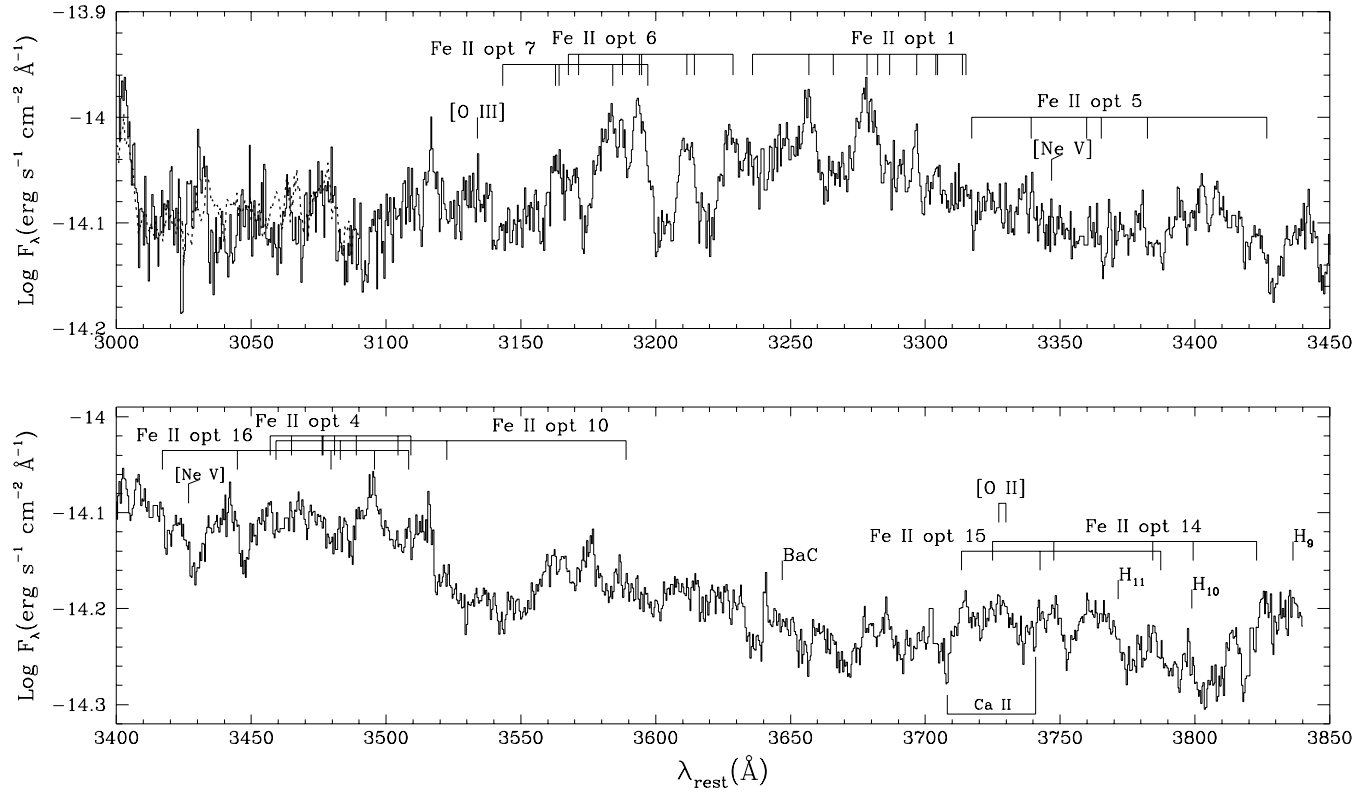
Fe II opt 7
Fe II opt 6
Fe II opt 1
[O III]
Fe II opt 5
[Ne V]
Log F$_\lambda$(erg s^{-1} cm^{-2} Å^{-1})
Fe II opt 16
Fe II opt 4
Fe II opt 10
[Ne V]
[O II]
Fe II opt 15
Fe II opt 14
BaC
H$_{11}$
H$_{10}$
H$_9$
Ca II
λ_{rest}(Å)

FIG. 2*d*

TABLE 1

EMISSION-LINE PARAMETERS

$\lambda_{obs}/(1+z)$ (Å)	λ_{ID} (Å)	Ion	Flux[a]	EW (Å)	FWHM (km s^{-1})	ΔV (km s^{-1})	Comments
1110–1130	1122 + ?	Fe III UV 1 + ?	31.1	12.6	...	...	
1174.9	1175.7	C III*	5.2	1.8	1210	−200	
1206.2	1206.5	Si III	...	...	...	−75	Affected by absorption on both sides
1214.2	1215.7	H I	382	128	1460	−370	N V subtraction is only approximate
1236.7, 1239.1	1238.8, 1242.8	N V	52	19	2350	−890	Velocity shift based on 1242.8 Å component
1249.5	1246.7, 1248.4, 1251.1	Si II*	...	...	...	...	Tentative identification
1260.5, 1264.5	1260.4, 1264.7, 1265.0	Si II	10.5	3.1	...	0	Strongly blended components
1302.6, 1305.5	1302.2, 1304.9, 1306.0	O I	20.6	8.3	...	0	Flux and EW for O I + Si II blend
1309.2	1304.4, 1309.3	Si II	20.6	8.3	...	0	As above
1334.3	1335.3	C II	8.8	3.6	1250	−220	
1344.3	?	?	2.2	0.9	1050	...	Unidentified
1392.1, 1400.6	1393.76, 1402.77	Si IV	47.7	17.4	...	−360	Flux and EW for Si IV + O IV] blend
	1401	O IV	47.7	17.4	...	...	As above
1543.4, 1546.0	1548.19, 1550.77	C IV	107	28.9	3930	−930	
1629.5	1640.4	He II	9	2.5	1700	−1990	Blended features at 1620 and 1640 Å?
	1660.81, 1666.15	O III]	8.3	2.5	...	...	Flux and EW for O III] + Al II blend
1670.5	1670.89	Al II	8.3	2.5	...	−70	Flux and EW for O III] + Al II blend
1746.9	1749.7	N III]	12.5	3.5	1800	−480	Broad multiplet (1746.82–1753.99 Å)
1785.8	1785.3, 1786.7, 1788.0	Fe II UV 191	4.8	1.4	910	−150	Approximate shift
1807.9, 1816.2	1808.01, 1816.93, 1817.45	Si II	5.0	1.5	...	0	
1852.7, 1860.8	1854.72, 1862.79	Al III	16	4.4	...	−320	Blended features at 1840 and 1870 Å
1881.1	1882.7	[Si III]?	...	...	...	−250	Marginal detection
1890.9	1892.03	Si III]	32.5	9.1	...	−250	Blended with C III]
1894.0	1895.46	Fe III UV 34	...	...	...	−230	Marginal detection
1906.4	1906.68	[C III]?	...	...	...	−40	As above
1907.8	1908.73	C III]	17.7	5.1	...	−150	Flux and EW for the C III] + Fe III UV 34 1914 blend
1912.6	1914.06	Fe III UV 34	17.7	5.1	...	−230	As above
1924.4	1926.30	Fe III UV 34	7.6	2.2	...	−300	
1951.7	1951.0, 1952.6, 1953.3	Fe III UV 68	5.7	1.8	...	−140	Shift relative to central component
2060.3, 2067.2	2062.20, 2068.90	Fe III UV 48	6.2	2.0	...	−260	
2078.9	2079.65	Fe III UV 48	1.4	0.5	640	−110	
2141.4	2139.68, 2143.45	N II]	6.5	2.6	1540	−90	
2325.8	2324.21, 2328.84	C II]	6.3	2.1	810	−90	
2418.9	2419.3, 2438.9	Fe III UV 47	7.8	2.6	720	−450	Identification as [Ne IV] λλ2422, 2425 unlikely
2668.6	2669.95	Al II]	3.0	1.2	900	−150	
2797.4, 2802.4	2796.35, 2803.53	Mg II	52.1	18.9	1600	0	FWHM affected by blending

NOTE.—The mean multiplet wavelength, instead of individual components, is listed if velocity separation is smaller than ∼300 km s^{-1}, or if more than three components are present.

[a] Flux is in units of 10^{-14} ergs s^{-1} cm^{-2}.

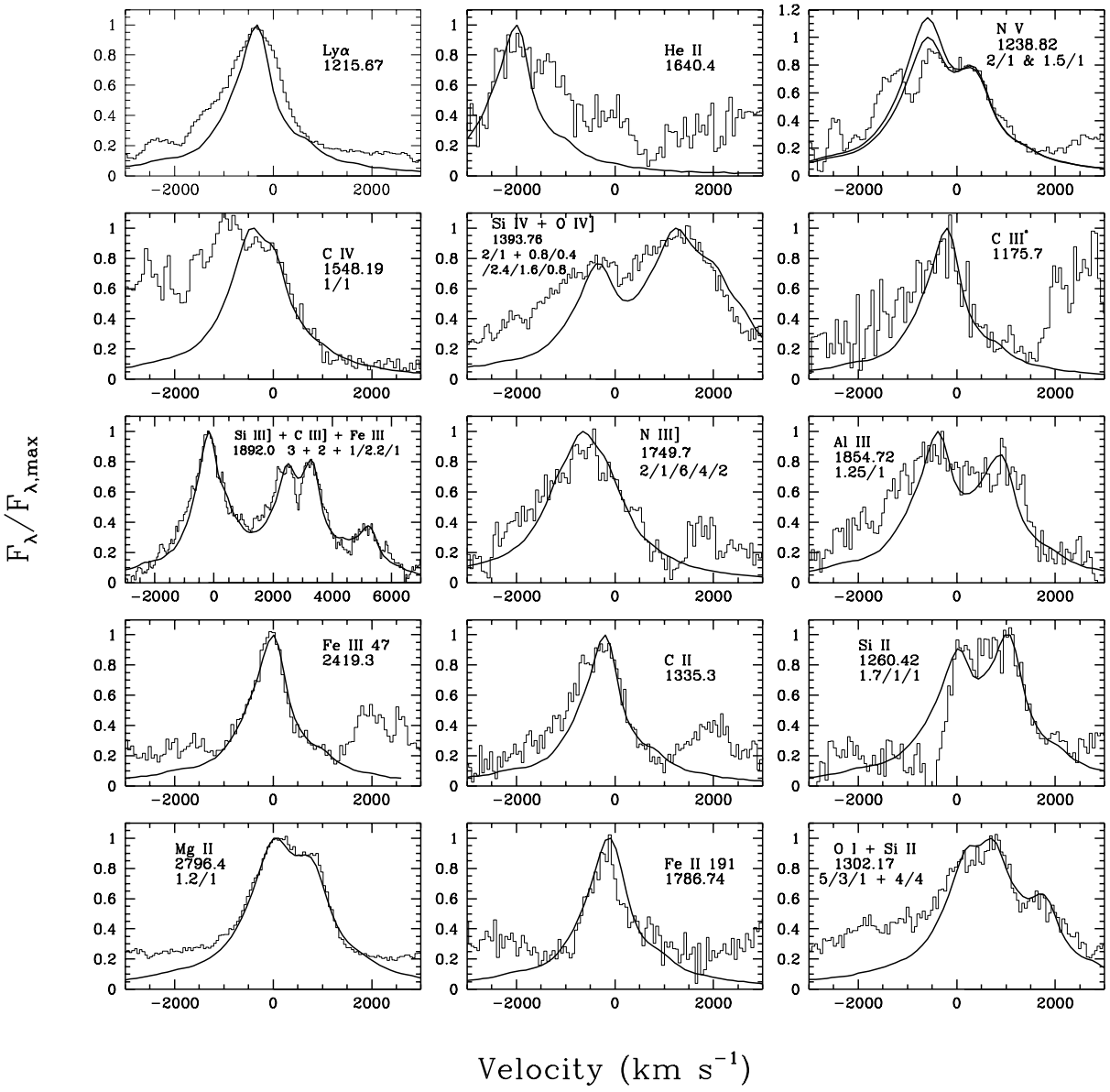

FIG. 3.—Emission-line profiles for selected lines observed in the spectrum of I Zw 1. The histogram represents the observed profile, and the solid line is the Hα profile fit. Multiplets are fit with a sum of template components. The wavelength used to set the velocity scale, and the multiplet component flux ratios are indicated in each panel. Note the overall bad fit and large velocity shifts of the high-ionization lines (*upper panels*) and the much better fit and very small shifts of the low-ionization lines (*lower panels*).

deduced from the neutral hydrogen column density of $N_{\rm H\,I} = 5.07 \times 10^{21}$ cm^{-2} taken from Elvis, Lockman, & Wilkes (1989) and the relation $E(B-V) = N_{\rm H}/4.93 \times 10^{21}$ found by Diplas & Savage (1994). The rest wavelength was calculated assuming $z = 0.0608$, the redshift of Hα and Hβ (e.g., Phillips 1976). A composite spectrum of ~700 quasars observed from the ground by Francis et al. (1991, hereafter the Francis et al. composite) is also shown for comparison. This composite represents well the "average" quasar's continuum and matches well similar composites constructed for lower z quasars with *HST* (see Fig. 2 in Laor et al. 1995).

The optical spectrum of I Zw 1 displayed in Figure 1 was kindly provided by B. Wills (1996, private communication). It matches the *HST* spectrum in the overlap region, 3170–3270 Å, to better than 5% and is used here to demonstrate the overall spectral shape. A flux discontinuity may be present just blueward of C IV (log $\nu = 15.29$) since the region at log $\nu > 15.29$ (obtained with the G190H) was observed 7 months after the log $\nu < 15.29$ region (obtained with the G130H). The overall optical-UV power-law slope is $\alpha \approx -1$, significantly redder than the slope of the typical quasar ($\alpha \approx -0.3$, as displayed by the Francis et al. composite or other optically selected samples, e.g., Neugebauer et al. 1987). This may indicate that I Zw 1 is significantly reddened, as further discussed in § 3.3. Note that many weak features in the Francis et al. composite are seen in I Zw 1 as clear and well-resolved lines.

Figures 2*a*–2*c* present an expanded view of the UV spectrum shown in Figure 1. The rest-frame positions of various lines are marked above the spectrum. Lines marked below the spectrum designate various absorption lines originating in the Galactic interstellar medium. All ISM lines detected

here are typically seen in FOS spectra of quasars (Savage et al. 1993). We make no attempt here to identify the many Fe II emission blends present. The various Fe II multiplets designated in Figure 2 are taken from Moore (1952) and serve only as an illustration of possible Fe II features. The number of possible Fe II multiplets is extremely large, and a reliable identification requires detailed theoretical calculations, which are beyond the scope of this paper.

Figure 2*d* presents the optical spectrum. The spectrum was obtained in a single exposure and is affected by cosmic-ray hits, which were deleted by taking out five small patches (width of 1–2 Å) from the spectrum. The absolute flux calibration is not secure. The wavelength zero point was set using Ca II $\lambda\lambda$3934.78, 3969.59 Galactic interstellar medium absorption lines. Since the *HST* wavelength zero point is also based on low-ionization species (Si II, Al II, Fe II), it probably matches well the optical spectrum zero point. The *HST* FOS G270H spectrum that overlaps with the optical spectrum in the 3183–3280 Å region is also shown in Figure 2*d*, shifted down by a factor of 0.37 in log flux. Apart from the flux discrepancy, the spectral features match very well. All the optical Fe II multiplets from the first 20 optical Fe II multiplets listed by Moore (1959) are marked for illustration only (it does appear though that some of the observed lines agree with expected positions). Note the absence of the [O II] λ3727 and [Ne V] $\lambda\lambda$3346, 3426 forbidden lines.

Table 1 lists for each emission feature the measured rest-frame wavelength (defined as the wavelength of the peak flux in the Gaussian smoothed spectrum), the expected wavelength, the emitting ion, the observed flux, rest-frame equivalent width, full width at half-maximum (FWHM), and the velocity shift of the peak of the emission line. These parameters were measured by fitting a set of Gaussians to each emission feature, as described in Laor et al. (1994a, 1995). In strongly blended features, or in very weak features, some of the emission parameters could not be measured reliably and are therefore not listed. We preferred not to assign errors to the measured parameters since such errors may not be very meaningful given the very complicated overall spectrum and the subjectivity of both the placement of the continuum and separation of blended features.

Figure 3 presents a comparison of an Hα profile with the observed profile of most of the strong emission features. Direct comparison of line profiles is not meaningful in most cases since most lines are strongly blended (despite their narrow profile in I Zw 1). The comparison is therefore made using a template profile, which allows us to test if the observed profile can be reconstructed with a sum of template components representing the various lines that may contribute to the blend. For the template we use the high S/N spectrum of Hα obtained for I Zw 1 as part of the BG92 study. The Hα line is used since it has the highest S/N and is the least blended. The wavelength used to set the velocity scale is given in each subpanel. Most features are blends, and in each subpanel we list the ratio of fluxes in the blend components assumed in the fit. When searching for the best fit, we allowed the continuum level to be below the apparent continuum level, since the observed continuum may be contaminated by weak unresolved emission (see in particular the Mg II doublet fit, discussed in § 3.1.5). Note that the Hα profile is slightly asymmetric with some excess flux on the blue wing (e.g., see the C IV 1/1 doublet fit). The template fits were not used for measuring any of the emission-line parameters.

3. EMISSION LINES

Below we describe some of the BLR diagnostics provided by ratios of lines from different levels of a given ion or within certain multiplets of a given ion.

3.1. *Line Diagnostics*

3.1.1. He

The $R_{\rm He\,II} \equiv$ He II λ4686/He II λ1640 flux ratio can be used as a reddening indicator. Below we explore its usefulness in I Zw 1. There is a very weak feature, if any, at the expected He II rest wavelength of 1640.4 Å. The nearest strong feature is at 1629.5 Å, which we suggest is highly blueshifted ($\sim$2000 km s^{-1}) He II emission. Alternatively, this feature may be just another Fe II feature, many of which are scattered throughout the spectrum. However, we find the He II identification more likely since C IV and N V also display large blueshifts ($\sim$900 km s^{-1}), and the He II velocity shift is typically twice that of C IV (e.g., Laor et al. 1995, Table 7). In addition, the He II/Lyα flux ratio of $\sim$0.03 measured using the 1629.5 Å feature is typical of quasars (e.g., Laor et al. 1995, Table 6).

Photoionization models indicate values of about $R_{\rm He\,II} \simeq$ 8–11 (Netzer, Elitzur, & Ferland 1985). BG92 did not detect the He II λ4686 line. A plausible upper limit on the EW is 0.5 Å using the BG92 high S/N optical spectrum, which implies a line flux less than 5×10^{15} ergs s^{-1} cm^{-2} Å^{-1}, where the continuum flux level is obtained from a lower resolution optical spectrum presented in Figure 1. We thus get $R_{\rm He\,II} > 18$. However, since the He II λ1640 line is very broad and asymmetric, the He II λ4686 upper limit may have been somewhat underestimated, while some of the flux attributed to He II λ1640 may be due to blended Fe II features. Therefore, the $R_{\rm He\,II}$ does not provide a useful constraint on the reddening.

3.1.2. C

Metal lines are produced mostly by collisional excitation of ions in their ground level. The C III* λ1176 line discussed below is unique in that it originates from radiative decay between two relatively high-lying levels. The transition is from the $2p^2\ ^3P$ level, 17 eV above the ground level, down to the metastable $2s2p\ ^3P$ level, 6.5 eV above the ground level (which decays to ground level via the C III] λ1909 line). The typical temperature in the C III region in photoionized gas is less than 2×10^4 K, and the small Boltzmann factor, $e^{-\chi/kT} < 5 \times 10^{-5}$ ($\chi = 17$ eV), suggests that the collisional excitation rate would be low and therefore that the line flux should be small.

The C III* λ1176 line is clearly detected in I Zw 1. The presence of this line was already suggested by Laor et al. (1995, Fig. 4) in high S/N FOS spectra of PG 1116+215, PG 1216+069, and PG 1538+477, but these detections were only marginal because of the effects of absorption by the Lyα forest and because of strong blending with the Lyα blue wing. These two effects are negligible in I Zw 1, and the line can therefore be clearly detected. The C III* λ1176/Lyα flux ratio found in those three objects is 0.02–0.05 versus a comparable ratio of 0.014 found here. This line was also detected recently in a composite *HST* spectrum of quasars at a similar level (Hamann et al. 1997).

Laor et al. (1997b) briefly discussed various excitation mechanisms for C III* λ1176 and showed that the observed high C III* λ1176/C III] λ1909 flux ratio is $\sim$50 times larger

than expected if collisional excitation at typical BLR conditions is the only significant process. However, as discussed below, the BLR density in the C III region of I Zw 1 is probably about an order of magnitude larger than in a typical BLR, which strongly suppresses C III] λ1909 emission. In addition, the gas temperature in the BLR tends to increase with increasing density (due to thermalization of some of the main coolants), which increases the C III* λ1176 emission, as shown by Korista et al. (1997, their Fig. 3*c*). The suppression of C III] λ1909 and enhancement of C III* λ1176 at $n_e \gtrsim 10^{11}$ cm^{-3} can explain the high C III* λ1176/C III] λ1909 flux ratio in I Zw 1. Note that dielectronic recombination (Storey 1981) also contributes significantly to the C III* λ1176 flux. Laor et al. (1997b) suggested that dielectronic recombination is not significant in I Zw 1 based on the C III λ2297 line flux, but this suggestion was based on a misquote of Storey (1981), and the actual values do not rule out a significant contribution from dielectronic recombination. Resonance scattering of continuum photons may also contribute significantly to the C III* λ1176 emission if the velocity dispersion within the BLR clouds is large enough (Ferguson, Ferland, & Pradhan 1995; Laor et al. 1997b).

The [C III] λ1907 line may be present in I Zw 1. This line is produced by a forbidden transition from the $^3P_2$ term in the 2*s*2*p* configuration of C III down to the ground level, with a critical density of $n_c = 5 \times 10^5$ cm^{-3} (Osterbrock 1989, Table 3.11). The $^3P_2$ term lies 0.007 eV above the $^3P_1$ term, which produces the well-known C III] λ1909 line, where $n_c \sim 5 \times 10^9$ cm^{-3}. Thus, the flux ratio $R_{\rm C\,III} \equiv$ [C III] λ1907/C III] λ1909 provides a temperature-independent density diagnostic (e.g., Osterbrock 1989, Fig. 5.5).

The observed C III] λ1909 line profile appears to be double peaked, with the short wavelength peak at 1906.4 Å, matching well the expected 1906.68 Å position of the [C III] line. This identification is not secure since excess emission is seen on the blue side of some of the other emission lines (see § 3.2), and the significance of the feature is only marginal. But, an analogous [Si III] λ1883 line may also be present (see § 3.1.7), which implies similar conditions. If true, then the [C III] line is much narrower and weaker than the C III] line. The observed $R_{\rm C\,III} \lesssim 0.1$ then implies that some of the C III emission originates in gas with an electron density of $n_e \lesssim 5 \times 10^5$ cm^{-3}.

The only clear detection of the [C III] λ1907 line in AGNs is apparent in the high-dispersion *IUE* spectrum of NGC 4151 displayed by Bromage et al. (1985, Fig. 1).

The C III] λ1909 line is very weak in I Zw 1. Both its EW of ∼2.5 Å and the C III]λ1909/Lyα = 0.023 flux ratio are a factor of 5–10 smaller than typically observed (e.g., Francis et al. 1991; Laor et al. 1995; Wills et al. 1995). Since C III] λ1909 is thermalized at $n_e \gtrsim 5 \times 10^9$ cm^{-3}, the suppression of C III] λ1909 may imply that the typical BLR density in I Zw 1 is about an order of magnitude larger than indicated by C III] λ1909 in typical AGNs, i.e., $n_e \sim 10^{11}$ cm^{-3} instead of $n_e \sim 10^{10}$ cm^{-3}. Additional evidence for this interpretation is provided by the Si III] λ1892 line discussed in § 3.1.7.

3.1.3. N

The N V λλ1239, 1243 doublet components are separated by the equivalent of ∼1000 km s^{-1}, and the narrow-line profiles in I Zw 1 suggest that this doublet should be resolvable. However, the N V profile shows a large excess flux at the blue wing, and the Hα template fit is inadequate (see Fig. 3). It does appear, however, that the doublet flux ratio is significantly lower than the optically thin 2/1 ratio. The physical implication of the observed doublet ratio is discussed below for the Mg II and Al III doublets, which are rather well resolved (§§ 3.1.5, 3.1.6).

3.1.4. O

The O I λ1304 line is thought to be produced through Bowen fluorescence. In this process, a Lyβ (1025.72 Å) photon is absorbed by O I in the ground 2*p* ^3P level and gets excited to the 3*d* ^3D level, which is within the thermal core of Lyβ (1025.77 Å). The decay back to the ground level is either direct or through two intermediate levels. The indirect decay route results in a λ11287 photon (3*d* ^3D to 3*p* ^3P), a λ8446 photon (3*p* ^3P to 3*s* ^3S), and a λ1304 photon (3*s* ^3S to 2*p* ^3P). Thus, one expects equal number of photons in these three lines. Rudy, Rossano, & Puetter (1989) very nicely confirmed this prediction for the λ11287 and λ8446 lines in I Zw 1. Below we show that the same number of photons is not seen in the λ1304 line and briefly discuss possible implications.

The O I λ1304 line is blended with the Si II λλ1304, 1309 doublet. This blending is very strong in most quasars, preventing a reliable estimate of the relative contributions of O I and Si II to the blend even in studies of high-quality spectra dedicated to Si II (e.g., Appendix A in Baldwin et al. 1996). In I Zw 1 the Si II λ1309 component of the Si II doublet is clearly resolved. The Si II λ1304 component is hopelessly blended with the O I λ1304 line, which is actually a triplet at 1302.17, 1304.86, and 1306.0 Å. However, the Si II 1309/1304 flux ratio should either be 2/1 (optically thin case) or 1/1 (optically thick case), and thus the clear detection of the 1309 component allows an estimate of the 1304 component flux within a factor of 2. The template fit to the O I + Si II blend (Fig. 3), which assumes an optically thick Si II doublet, suggests that 0.5 of the blend flux is due to O I. If the Si II doublet is optically thin (less likely given the results in §§ 3.1.5, 3.1.6), then the Si II λ1304 component is only half as strong, and then 0.56 of the blend flux is due to O I. Using the O I λ8446 flux from Rudy et al. then gives $R_{\rm O\,I} \equiv$ λ8446/λ1304 photon flux ratio as 5.5 (4.8) for the optically thick (thin) case.

The shortest wavelength flux in the spectrum from which the Rudy et al. O I λ8446 flux is taken (at 7500 Å) agrees within ∼20% of the flux in the optical spectrum shown in Figure 1; thus, variability between the times the λ8446 and the λ1304 lines were measured is most likely not a significant source of error.

Kwan & Krolik (1981) have found that $R_{\rm O\,I}$ can increase from unity to 1.3 because of Balmer continuum absorption of λ1304 photons and the production of λ8446 photons by collisional excitation of O I ions in the 3*s*^3S level. A third mechanism that can increase $R_{\rm O\,I}$, noted by Grandi (1983), is the significant probability for a 2*p*^{4} ^1D–3*s* ^3S λ1641 semiforbidden transition for $\tau_{\lambda 1304} \geq 10^5$, or equivalently, $\tau_{\rm Ly\alpha} \geq 10^9$, which would further increase $R_{\rm O\,I}$. Kwan (1984) included the O I] λ1641 transition and indeed found $R_{\rm O\,I} \sim 3.2$, where most of the increase from unity is due to the "rerouting" of λ1304 photons to λ1641.

This mechanism can be tested in I Zw 1 since the He II λ1640 line is strongly blueshifted (to ∼1630 Å), while the O I lines are not. This allows us to look for the O I] λ1641

line and test if it can indeed explain the very high $R_{\rm O\,I}$ observed. No strong line is detected at 1641 Å, and we estimate that such a line cannot add more than $\sim 30\%$ to the observed $\lambda 1304$ line. The absence of a significant flux in the O I] $\lambda 1641$ line therefore implies that most of the Lyβ absorption by O I in I Zw 1 takes place at a depth where $\tau_{\rm Ly\alpha} < 10^9$.

Rudy et al. gave observational evidence that collisional excitations cannot significantly increase $R_{\rm O\,I}$ in I Zw 1. Thus, of the three mechanisms mentioned above, the only one left is Balmer continuum absorption of $\lambda 1304$ photons. It remains to be explored whether this mechanism can suppress the $\lambda 1304$ line by the required factor of ~ 5 when $\tau_{\rm Ly\alpha} < 10^9$.

Another option is that there are few O I $\lambda 1304$ photons because the observed emission is strongly reddened, as discussed below in § 3.3.

Another observed emission line from O is the O IV] $\lambda 1402$ line. This line is a multiplet of five components, and it is strongly blended with the Si IV $\lambda 1397$ doublet, producing a single broad $\lambda 1400$ feature in most AGNs. The relative contribution of O IV and Si IV has been debated in the past (Baldwin & Netzer 1978; Wills & Netzer 1979; Tytler & Fan 1992; Wills et al. 1993; Laor et al. 1994a). The narrow lines of I Zw 1 appear to provide a good opportunity to determine accurately the relative contribution of O IV and Si IV to the $\lambda 1400$ feature.

The peak of the $\lambda 1400$ blend is clearly split in I Zw 1 into two peaks at 1392.1 and 1400.6 Å. These correspond well to the expected positions of the Si IV doublet at 1393.76 and 1402.77 Å, blueshifted by ~ 2 Å. However, some O IV] must also be present based on the following argument. The 1392.1 Å feature must be due to Si IV only (the shortest wavelength O IV] component is at 1397.2 Å). The second Si IV doublet component is at 1400.6 Å, and its flux should either be equal to (optically thick) or half of (optically thin) the 1397.2 Å line flux. The observed 1400.6 Å component is stronger than the 1392.1 Å component and must therefore include some O IV] emission. A specific template deblending is shown in Figure 3, using Hα as a template, which implies a Si IV/O IV] flux ratio of $\frac{1}{2}$. However, this ratio is not well constrained since the intrinsic line profile is probably not symmetric, as suggested by the large observed blue excess flux, and the fact that all other high-ionization lines display a strong blue excess flux (see § 3.2). Thus, we can only verify that both Si IV and O IV] are present and that they have roughly comparable flux.

3.1.5. Mg

The Mg II ion is produced by photons above 7.646 eV and destroyed by photons above 15.035 eV; it therefore survives mostly in the partially ionized H region, where photons above 13.6 eV are blocked. The Mg II $\lambda 2798$ doublet is therefore a diagnostic of the conditions in the extended partially ionized layers inside the BLR clouds. The flux ratio of the Mg II 2796.35/2803.53 Å components indicates the optical depth in the line. Below we describe the observed flux ratio and discuss its implication.

The Mg II $\lambda 2798$ profile is clearly double peaked. Its core is well fit with a 1.2/1 ratio for the 2796.35/2803.53 Å doublet lines using the Hα profile as a template (Fig. 3). A good fit requires that the actual continuum level be placed 20% below the observed flux level at the apparent line base. This continuum level matches very well the continuum level inferred at 2800 Å from a linear interpolation of the continuum at 2650 and 3020 Å.

What does the 1.2/1 doublet ratio implies for the conditions in the Mg II emitting gas? The 2803.53, 2796.35 Å lines correspond to transitions from the $3p\ ^2P_{1/2}$ and $3p\ ^2P_{3/2}$ levels to the ground $3s\ ^2S_{1/2}$ level. The collision strength at $T = 10^4$ K is $\Omega(^2P, ^2S) = 16.9$ (Pradhan & Peng 1995), yielding collisional deexcitation rates of $q(3p\ ^2P_{3/2}, 3s\ ^2S_{1/2}) = 3.65 \times 10^{-7}$ and $q(3p\ ^2P_{1/2}, 3s\ ^2S_{1/2}) = 7.3 \times 10^{-7}$. The radiative deexcitation rates for the $3p\ ^2P_{3/2,1/2}$ levels are $A = 2.6 \times 10^8$ s^{-1} (Morton 1991). Collisional deexcitation dominates when

$$\tau_0 n_e > A/q ,$$

where τ_0 is the line-center optical depth for resonance scattering, i.e., when $\tau_0 n_e > 7.1 \times 10^{14}$ cm^{-3} and 3.6×10^{14} cm^{-3} for the $3p\ ^2P_{3/2}$ and $3p\ ^2P_{1/2}$ levels. For $\tau_0 n_e > 7.1 \times 10^{14}$ cm^{-3} the Mg II 2796.35/2803.53 Å doublet ratio is thermalized; i.e., it changes from 2/1 to 1/1 (see Hamann et al. 1995 for results on other analogous UV doublets). Thus, the observed 1.2/1 ratio implies that most of the Mg II emission is produced in a region where $\tau_0 n_e \gtrsim 10^{15}$ cm^{-3}.

What does the above result implies for the conditions in the partially ionized BLR gas? As shown below, the value of $\tau_0 n_e$ provides a direct measure of the distance of the BLR clouds from the central ionizing continuum source. The line-center optical depth is $\tau_0 = \sigma_{v_0} \Sigma_{\rm Mg\,II}$, where $\sigma_{v_0} = 1.47 \times 10^{-12}$ cm^2 is the total Mg II doublet line-center absorption cross section (for $T = 10^4$ K) and $\Sigma_{\rm Mg\,II}$ is the column density of Mg II ions. The partially ionized H region, where Mg II survives, has a column density about 10–30 times larger than the column density of the highly ionized H region, given by $\Sigma_{\rm H\,II} = 10^{23} U$ cm^{-2}, where U is the ionization parameter ($\equiv n_\gamma/n_e$, the photon/electron density). Balmer continuum absorption may limit the depth of the Mg II doublet emitting layer, but this absorption will not affect our conclusion. Using the Mg/H solar abundance ratio of 3.8×10^{-5}, and assuming most Mg is Mg II, we get $\Sigma_{\rm Mg\,II} \simeq 4 \times 10^{19} U$ cm^{-2}, or $\tau_0 = 6 \times 10^7 U$, assuming the gas is ionization, rather than matter bounded. The Mg II doublet is therefore thermalized when $6 \times 10^7 U n_e \gtrsim 10^{15}$, or $n_\gamma \gtrsim 10^7$ cm^{-3}.

Reverberation mapping (e.g., Netzer 1990; Peterson 1993; Maoz 1995; Kaspi et al. 1996), and theoretical considerations (Netzer & Laor 1993) suggest $R_{\rm BLR} = 0.1 L_{46}^{1/2}$ pc, which implies $n_\gamma \sim 2 \times 10^9$ cm^{-3} in the BLR. Thus, the observed 1.2/1 Mg II doublet ratio provides direct confirmation that the BLR is indeed optically thick in the Mg II $\lambda 2798$ line, as predicted by "standard" photoionization models for the BLR. More refined calculations using actual photoionization models can be used to explore the exact doublet ratio predicted by various BLR models and its agreement with the observed value.

Note that one generally expects a doublet ratio from optically thick gas to be somewhere between 2/1 and 1/1 rather than 1/1, since (as is always the case in atmospheres) most of the contribution to the line flux arises from the region where the emission just becomes optically thick, i.e., from the region where the doublet ratio changes from 2/1 to 1/1.

3.1.6. Al

The components of the Al III $\lambda 1857$ doublet are widely spaced (~ 1300 km s^{-1}) and are therefore clearly resolved in

I Zw 1. Al III is created by photons above 18.829 eV and destroyed by photons above 28.448 eV; thus, unlike Mg II, it exists in the highly ionized H region only, and the observed Al III doublet ratio provides constraints on the BLR H II region, as discussed below.

The template fit suggests a 1.25/1 ratio for the 1854.71/1862.79 Å doublet lines (Fig. 3). This ratio is somewhat uncertain since there are significant deviations from the Hα template fit, possibly due to blending with Fe II multiplets (e.g., Wills, Netzer, & Wills 1980) or an intrinsic blue excess flux, as displayed by other high-ionization lines (§ 3.2). Baldwin et al. (1996) found a similar 1/1 flux ratio in three objects where the Al III doublet was clearly detected.

Below we calculate the expected Al III λ1857 doublet ratio, as calculated above for the Mg II λ2798 doublet.

The Al III and Mg II ions are both Na I–like. Thus, the 1854.71 and 1862.79 Å Al III lines are also produced by transitions from the $3p\ ^2P_{1/2}$ and $3p\ ^2P_{3/2}$ levels to the ground $3s\ ^2S_{1/2}$ level. The collision strength at $T = 10^4$ K is $\Omega(^2P, {}^2S) = 16.0$ (Dufton & Kingston 1987), the radiative deexcitation rate is $A = 5.4 \times 10^8\ s^{-1}$ (Morton 1991), the solar Al/H abundance ratio is 3.6×10^{-6}, and $\sigma_{\nu_0} = 9.4 \times 10^{-13}$ cm^2. Al III exists in the highly ionized H region only, where $\Sigma_{H\,II} = 10^{23} U$ cm^{-2}. Using these parameters, and assuming Al is mostly Al III, we find that the Al III λ1857 doublet is thermalized for $n_\gamma \gtrsim 4 \times 10^9$ cm^{-3}.

The observed 1.25/1 Al III doublet ratio suggests that Al III is formed in clouds at, or inside, the "standard" BLR radius of $0.1 L_{46}^{1/2}$ pc, where $n_\gamma \gtrsim 2 \times 10^9$ cm^{-3}. The fact that the Al III doublet is expected to be only marginally thermalized at the "standard" BLR radius suggests that this doublet ratio can provide an interesting probe of the size of the BLR.

The relatively large Al III λ1857 EW (4.4 Å) requires a BLR component where Al III is the dominant ionization state of Al, which occurs for $U \sim 10^{-2}$–10^{-3} (e.g., Baldwin et al. 1996, Fig. 7*a*). Since $n_\gamma \gtrsim 4 \times 10^9$ cm^{-3}, the above range in U implies $n_e \gtrsim 4 \times 10^{11}$–$4 \times 10^{12}$ cm^{-3}, which is comparable to, or denser than, the component responsible for the C III] λ1909 emission (§ 3.1.2).

We caution that resonance scattering of continuum photons has not been included in the above discussion. This process could contribute an EW of ∼2 Å to each of the Al III λ1857 doublet components, i.e., as much as observed, if the velocity dispersion in the BLR clouds is as large as the lines FWHM and the clouds cover ≳30% of the continuum source (e.g., Ferguson et al. 1995). Continuum resonance scattering would also imply a much lower value for τ_0 than estimated above (due to the large velocity gradients required in the BLR clouds). Calculations with detailed photoionization codes are required in order to understand whether continuum resonance scattering is indeed viable.

3.1.7. Si

The Si II 1260.42, 1264.74, 1265.00, 1304.37, 1309.28, 1808.01, 1816.93, and 1817.45 Å lines are clearly detected. The flux of the Si II λ1194 and λ2335 blends is well constrained. This wealth of data provides a unique opportunity to explore the Si II line formation mechanisms (e.g., Baldwin et al. 1996, Appendix C). Such analysis is beyond the scope of this paper.

The outer shell electronic configuration of the Si III ion is analogous to that of C III. The analogous line to the [C III] λ1907 line (§ 3.1.2) is the [Si III] λ1883 line, which can also be used as a density diagnostic for the Si III gas. Weak [Si III] λ1883 emission may be present at 1881.1 Å. The identification of this marginal feature is supported by the fact that its 250 km s^{-1} blueshift matches the Si III] λ1892 shift and by the possible presence of the analogous [C III] λ1907 line. As for the C III ion, the $R_{Si\,III} \equiv$ [Si III] λ1883/Si III] λ1892 flux ratio is a robust density indicator (Keenan, Feibelman, & Berrington 1992). The observed $R_{Si\,III} \lesssim 0.1$ implies that some of the Si III resides in gas with $n_e \sim 5 \times 10^5$ cm^{-3}, i.e., the same conditions implied by $R_{C\,III}$, as expected since the spatial distribution of both ions in photoionized gas should largely overlap.

The Si III] λ1892/C III] λ1909 flux ratio of ∼3.5 is significantly larger than the typical ratio of $\sim 0.3 \pm 0.1$ observed in quasars (Laor et al. 1995). This high ratio results from the factor of 5–10 suppression in the C III] λ1909 flux (§ 3.1.2), rather than significant enhancement of Si III] λ1892. The most likely interpretation for this high ratio is a relatively dense BLR. The critical density for C III] λ1909, $n_C \sim 5 \times 10^9$ cm^{-3}, is significantly smaller than for Si III] λ1892, where $n_C = 1.1 \times 10^{11}$ cm^{-3}. Thus, if the BLR density is 10^{11} cm^{-3}, rather than 10^{10} cm^{-3}, C III] λ1909 would be suppressed by a factor of ∼10, while Si III] λ1892 would not be affected, consistent with our observations.

3.1.8. Fe

The positions of some Fe II UV blends are marked in Figure 1 only to illustrate various possible Fe II emission features. Numerous additional weak Fe II blends are most likely present at other wavelengths. Because of the extreme complexity of the Fe II ion, we do not attempt to identify individual features.

The likely presence of Fe II emission well below 2000 Å, and possibly even at ∼1110–1130 Å, indicates that Fe II is excited by processes other than just collisions, as the electron temperature in the Fe II region is most likely far too low for significant collisional excitation of levels ≳10 eV above the ground state. One such process, suggested by Penston (1987), is resonance absorption of Lyα photons by Fe II. Johansson & Jordan (1984) found Lyα resonance absorption to be significant in various stellar systems and identified Fe II λ1294, Fe II UV 191 λ1787, and the Fe II λ1871 multiplets as the signatures of such a process (see also Johansson & Hamann 1993). The Fe II UV 191 multiplet is very prominent in I Zw 1, and weak emission blends are clearly apparent at 1294, and 1870 Å, suggesting that resonance absorption of Lyα photons may be a significant excitation mechanism for Fe II in I Zw 1 as well. Resonance scattering of continuum photons and Fe II–Fe II line fluorescence could also be a significant process for populating high-lying Fe II levels (e.g., Netzer & Wills 1983; Wills, Netzer, & Wills 1985). Clearly, the Fe II–rich spectrum of I Zw 1 should serve as a valuable tool for future studies of Fe II emission in AGNs.

A number of Fe III multiplets are clearly present. The Fe III UV 34 multiplet, clearly identified here, was first discovered by Hartig & Baldwin (1986) in a broad absorption line quasar. An emission feature near ∼2070 Å is commonly seen in quasars (e.g., Wills et al. 1980), and was identified as a likely Fe II blend. Baldwin et al. (1996) suggested that this feature is due to Fe III UV 48 emission. Here the three Fe III UV 48 components at 2062.2, 2068.9, and 2079.65 Å are clearly resolved, which verifies the identity of this feature. The Fe III UV 47 λλ2419.3, 2438.9 doublet is

most likely present as well. Other Fe III blends, such as Fe III UV 50 and Fe III UV 68, and in particular the resonance Fe III UV 1 at 1122–1130 Å, may also be present, but these identifications cannot be verified here since these blends are not clearly resolved.

The relative flux ratio of the multiplet components can provide an important diagnostic for the optical depth and excitation mechanism of Fe III. Given the complexity of the Fe III ion, these diagnostics are beyond the scope of this paper.

3.2. *Line Profiles and Velocity Shifts*

Optical spectra of I Zw 1 revealed two velocity systems. The first system is at $z = 0.0608$ for the low-ionization forbidden lines and Balmer lines, including Hα; Hβ; optical Fe II multiplets; [Ca II] $\lambda\lambda$7291.46, 7323.89; [S II] $\lambda\lambda$4068.60, 4076.35; [N II] λ5754.57; He I λ5875.6; Na I $\lambda\lambda$5889.95, 5895.92; and [O I] $\lambda\lambda$6300.3, 6363.8. The second system is at $z = 0.0587$ (i.e., blueshifted by $\sim$630 km s^{-1}) for the higher ionization forbidden lines, [O III] $\lambda\lambda$4958.82, 5006.85 and [Ne III] $\lambda\lambda$3868.74, 3967.47 (Phillips 1976; Oke & Lauer 1979).

We find the same trend in the UV. As shown in Table 1, the low-ionization permitted lines, including O I λ1304; C II λ1335.3 and C II] $\lambda\lambda$2324.21, 2328.84; N II] $\lambda\lambda$2139.68, 2143.45; Al II λ1670.89 and Al II] λ2669.95; the various Si II multiplets; and Fe II 191 λ1787, are all blueshifted by $\lesssim$200 km s^{-1} with respect to $z = 0.0608$. Note that shifts of $\lesssim$100 km s^{-1} are consistent with zero shift, given the accuracy of our wavelength zero-point calibration using the interstellar medium lines. Higher ionization lines, including N III] λ1750; Al III $\lambda\lambda$1854.72, 1862.79; Si III] λ1892.03 and Si IV $\lambda\lambda$1393.76, 1402.77, are blueshifted by $\sim$300–500 km s^{-1}, while the highest ionization lines C IV $\lambda\lambda$1548.19, 1550.77 and N V $\lambda\lambda$1238.8, 1242.8, are blueshifted by $\sim$900 km s^{-1}. The highest blueshift, $\sim$2000 km s^{-1}, is displayed by He II λ1640.4.

This trend of increasing blueshift with increasing ionization level is observed in most quasars (e.g., Gaskell 1982; Wilkes 1984, 1986; Uomoto 1984; Espey et al. 1989; Corbin 1990). However, the typical amplitude of the high-ionization-line blueshift, such as C IV and N V, is only $\sim$200–300 km s^{-1}, and for He II it is $\sim$500 km s^{-1} (Tytler & Fan 1992; Laor et al. 1995), i.e., about 4 times lower than found in I Zw 1.

The low-ionization-line profiles are mostly consistent with the rather symmetric Hα profile. With increasing blueshift the lines get progressively broader and develop a progressively stronger blue excess asymmetry (see Fig. 3).

3.3. *Reddening*

As shown in Figure 1, the optical-UV spectrum of I Zw 1 is significantly redder than observed in typical quasars. Could the intrinsic continuum of I Zw 1 be similar to the Francis et al. composite, and could the observed red continuum just be due to reddening?

Intrinsic reddening by Galactic-like dust is ruled out as it would have produced a very pronounced broad absorption feature at 1800–2500 Å, which is not observed. The grain size distribution in AGNs may, however, be different than that in the Galactic ISM (e.g., Laor & Draine 1993), and in particular it may not produce a significant 2200 Å extinction bump. Thus, we cannot securely rule out reddening based on just the absence of the 2200 Å feature.

Reddening would also affect various optical/UV line ratios. In particular, assuming the correct optical/UV flux distribution is given by the Francis et al. composite implies that $R_{\rm O\,I} \sim 1.2$ (instead of 5.5), which is consistent with the value predicted by the Kwan & Krolik (1981) calculation (which does not include the production of a O I] λ1641, shown here to be insignificant). Dereddening also affects the Lyα/Hβ flux ratio. The intrinsic ratio would then be 32 instead of 7.6. Such a high Lyα/Hβ ratio is theoretically possible for plausible BLR parameters (e.g., Netzer et al. 1995), but it is much higher than the ratio of 5–15 typically observed in quasars.

If the intrinsic continuum of I Zw 1 is similar to the Francis et al. composite, and the observed continuum is due to reddening by Galactic-like dust (except the 2200 Å bump) intrinsic to I Zw 1, then the implied reddening is of $E(B-V) \sim 0.2$. For a Galactic dust/gas ratio this implies $N_{\rm H} = 10^{21}$ cm^{-2}. The *ROSAT* PSPC spectrum of I Zw 1 implies an intrinsic neutral column density of no more than $1.5 \pm 0.7 \times 10^{20}$ cm^{-2} (see § 4.2). Thus, the gas associated with the dust must either be highly ionized ($U > 1$), to prevent strong X-ray absorption below 0.4 keV, or the dust/gas ratio needs to be at least 5 times larger than the Galactic value. The X-ray absorption by the grain component itself is negligible at the above columns (see Fig. 6 in Laor & Draine 1993) and therefore cannot be used to constrain the dust column.

A nearly featureless X-ray power law may still be associated with a large dust column density along the line of sight if most of the observed X-rays are electron-scattered by an extended medium. In this case only a small fraction of the X-rays would be scattered, and thus although the X-ray power law would be featureless, its normalization relative to the optical would be significantly reduced. However, Lawrence et al. (1997) find an optical to X-ray power law of $\alpha_{\rm ox} = -1.41$, which is very close to the average value of $\alpha_{\rm ox} = -1.48$ for radio-quiet quasars (Laor et al. 1997a). Thus, it appears most likely that the primary X-ray source in I Zw 1 is observed directly, unless the direct optical flux is also completely obscured.

Theoretical and observational uncertainties therefore do not allow us to clearly conclude whether I Zw 1 is reddened or not.

4. INTRINSIC ABSORPTION

In this section we describe observational evidence for associated UV absorption and the implied constraints on the absorber column. We also discuss constraints based on the soft X-ray spectrum and a possible relation of the absorber to a highly blueshifted emission component.

4.1. *UV Absorption*

4.1.1. *Observational Evidence*

Figure 4 displays evidence for associated absorption in Lyα, N V, and C IV. The clearest evidence for absorption is seen in the N V $\lambda\lambda$1238.8, 1242.8 doublet. The N V absorption doublet is blueshifted by $\sim$1870 km s^{-1} relative to the $z = 0.0608$ frame; it has a FWHM $\sim$ 300 km s^{-1} and an absorption EW of $\sim$0.25 Å (determined using the λ1242.8 component). Since the spectral resolution of the FOS at N V is $\sim$230 km s^{-1}, the absorption system may not be truly resolved. The C IV $\lambda\lambda$1548.19, 1550.77 profile is consistent with having a very similar absorption system, although the

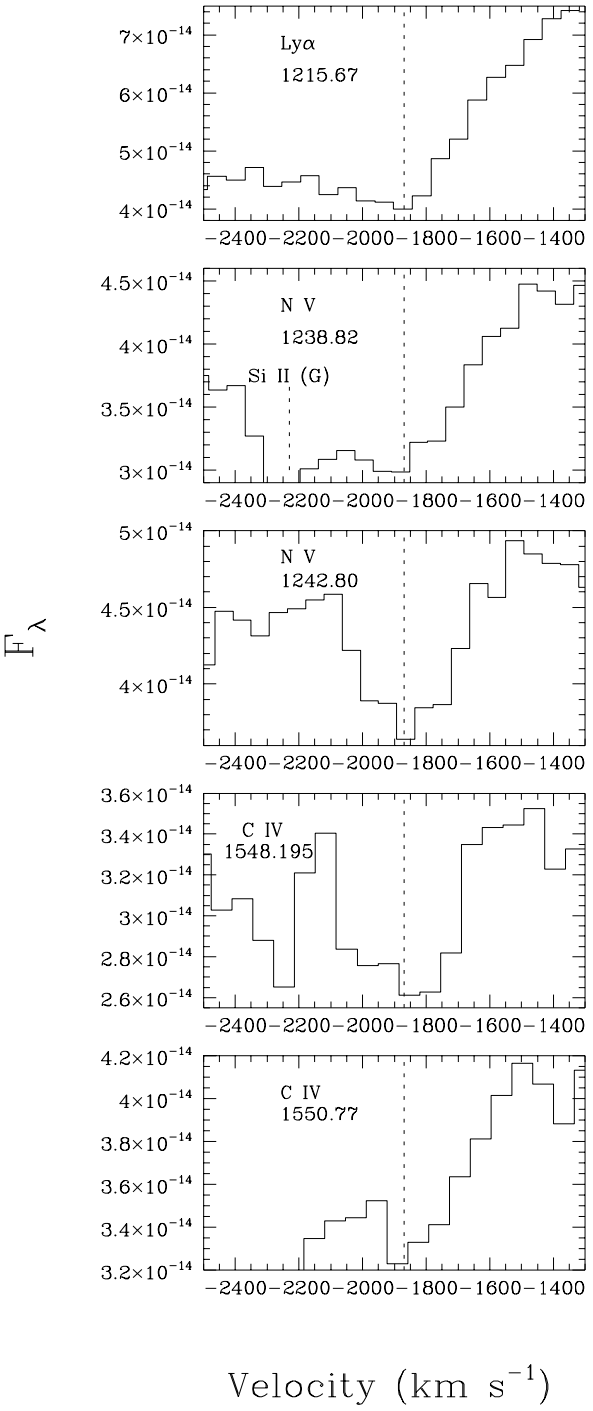

FIG. 4.—Absorption-line profiles of the candidate intrinsic UV absorption-line system. The rest wavelength used to set the velocity scale is indicated in each panel. The strongest evidence for absorption is seen in the N v λ1242.80 profile. The other lines are consistent with having absorption of similar EW and FWHM at the same velocity shift of ~1870 km s^{-1}.

spectrum has a very low S/N at the blue wing of C IV (it falls on the blue edge of the G190H). The Lyα profile appears to be affected by an absorption system with the same velocity shift and about the same EW and FWHM.

The presence of high-ionization lines, and lack of low-ionization lines, suggests the absorber is associated with I Zw 1 rather than with an intervening system unrelated to I Zw 1 (see, e.g., Hamann 1997). Most of the constraints below are independent of the exact location of the absorber.

4.1.2. *Implied Constraints*

The column density associated with the observed absorption EW is a function of the absorber optical depth. The optical depth can be deduced from the ratio of the EW of the two doublet components, even when the absorption-line profiles are not resolved, assuming the absorber completely covers the emission source. In the optically thin limit this ratio equals the ratio of oscillator strengths, i.e., EW(1238.8)/EW(1242.8) = 2, and when both absorption lines are saturated this ratio approaches unity. The observed ratio is ~1.4, but it is rather uncertain since the 1242.8 Å component absorbs the line peak where the underlying emission is not clearly defined, and the 1238.8 Å component is partly blended with Galactic Si II λ1304.37 absorption. The absorption optical depth therefore remains uncertain.

In the optically thin limit the absorber column density is related to the EW through

$$N_{\rm abs} = 1.13 \times 10^{20} \lambda^{-2} f^{-1} \ {\rm EW \ cm^{-2}} ,$$

where λ, the absorption wavelength, and its EW are in units of Å and f is the oscillator strength. Using $f(1215.67) = 0.416$, $f(1550.77) = 0.095$, $f(1242.8) = 0.078$, and an absorption EW of 0.25 Å for all lines, we get $N_{\rm H\,I} = 4.6 \times 10^{13}$ cm^{-2}, $N_{\rm C\,IV} = 1.2 \times 10^{14}$ cm^{-2}, and $N_{\rm N\,V} = 2.3 \times 10^{14}$ cm^{-2}. These values are lower limits on the absorber columns.

The upper limits on the columns are obtained in the optically thick limit, i.e., when only thermal broadening is present. If the absorption line profile is not resolved, and only the absorption EW is given, then the deduced column density depends on whether the line is optically thick in the Doppler core only or whether it is also thick in the Lorentzian wings (i.e., "damped absorption"). The first case applies when

$$\mathrm{EW}/\Delta\lambda_{\rm D} \lesssim 6 ,$$

where

$$\Delta\lambda_{\rm D} = 4.285 \times 10^{-5} \lambda T_4^{1/2} A^{-1/2}$$

is the thermal line width in Å, $T = 10^4 T_4$ K, and A is the atomic weight. The absorber column density is then given by

$$N_{\rm abs} = 2 \times 10^{20} \lambda^{-2} f^{-1} \Delta\lambda_{\rm D} e^{({\rm EW}/2\Delta\lambda_{\rm D})^2} .$$

When absorption is dominated by the Lorentzian wings, i.e., when

$$EW/\Delta\lambda_{\rm D} \gtrsim 6 ,$$

the absorber column density is

$$N_{\rm abs} \simeq 3.35 \times 10^{39} \lambda^{-4} f^{-1} \Gamma^{-1} \ {\rm EW^2} ,$$

where Γ is the radiative decay rate ($\Gamma_{1215.67} = 6.265 \times 10^8$ s^{-1}, $\Gamma_{1550.77} = 2.64 \times 10^8$ s^{-1}, $\Gamma_{1242.80} = 3.387 \times 10^8$ s^{-1}). Assuming $T_4 = 2$, the typical temperature of photoionized gas where C IV or N V dominate, we get the maximum possible columns of $N_{\rm H\,I} = 4.3 \times 10^{14}$ cm^{-2} (where $\mathrm{EW}/\Delta\lambda_{\rm D} < 6$) $N_{\rm C\,IV} = 1.4 \times 10^{18}$ cm^{-2}, and $N_{\rm N\,V} = 3.3 \times 10^{18}$ cm^{-2} (in both cases $\mathrm{EW}/\Delta\lambda_{\rm D} > 6$). The H I column density upper limit is rather uncertain since a Doppler core absorption gives $N_{\rm abs} \propto e^{({\rm EW}/2\Delta\lambda_{\rm D})^2}$, and thus a likely ±30% error in the H I EW corresponds to an upper limit in the

range of 0.1–3.1 $\times 10^{15}$ cm^{-2}. The C IV and N V upper limits are uncertain by only a factor of $\lesssim 2$, since $N_{abs} \propto$ EW^2, when the Lorentzian wings dominate the absorption.

To infer the total H column density from the H I column density one needs to know the H ionization state. The H II/H I fraction in the absorbing gas is related to the ionization parameter through

$$N_{H\,II}/N_{H\,I} \simeq 2 \times 10^5 U$$

(e.g., Netzer 1990). Thus, the upper limit on the H column density is

$$N_H \simeq N_{H\,II} = (0.2\text{–}6) \times 10^{20} U \text{ cm}^{-2} .$$

The presence of N V and C IV ions suggests that the absorber has $U \sim 0.01$–1, thus the H column density upper limit is probably in the range $10^{17} \lesssim N_H \lesssim 6 \times 10^{20}$. If the absorber metal abundance is solar, then the above N_H implies metal columns upper limits of $3.6 \times 10^{13} \lesssim N_C \lesssim 2 \times 10^{17}$ and $10^{13} \lesssim N_N \lesssim 6.7 \times 10^{16}$. These values overlap with the directly determined constraints on the C IV and N V columns and suggests that significant fractions of C and N are indeed in the form of C IV and N V, consistent with the assumption of $U \sim 0.01$–1. Detection of O VI $\lambda\lambda$1031.93, 1037.63 absorption would allow a much tighter constraint on the absorber's U.

4.2. *Soft X-Ray Absorption*

In addition to the UV absorption lines, there may also be some soft X-ray absorption in I Zw 1. Boller et al. (1996) and Lawrence et al. (1997) fit a single power law to the *ROSAT* PSPC spectrum of I Zw 1 and find a best-fit column density of $N_{H\,I} = 6.5\text{–}6.7 \pm 0.7 \times 10^{20}$ cm^{-2} (90% error) versus a Galactic value of $5.0 \pm 0.1 \times 10^{20}$ cm^{-2} (Elvis et al. 1989), suggesting that there may be an intrinsic absorber in I Zw 1 with $N_H \sim 1.5\text{–}1.7 \pm 0.7 \times 10^{20}$ cm^{-2}. Lawrence et al. (1997) find that a fit including only Galactic absorption can be excluded with a confidence level greater than 99%.

The observed total column density in I Zw 1 is optically thick below 0.38 keV, where He dominates the opacity. Thus, the only direct constraint from *ROSAT* is for $N_{He\,I} \sim 1.5 \pm 0.7 \times 10^{19}$ cm^{-2}, assuming the cosmic $n_{He}/n_H = 0.1$ abundance. A $\sim$20% higher column density applies if most of He is He II, as deduced using the Verner & Yakovlev (1995) He I and He II absorption cross sections.

Associations of UV and X-ray absorbers with the same gas was claimed in 3C 351 (Mathur et al. 1994) and NGC 5548 (Mathur, Elvis, & Wilkes 1995) but disputed in NGC 3516 (Kriss et al. 1996a, 1996b). Can the UV and the X-ray absorption in I Zw 1 originate in the same absorber? In a cloud photoionized by a typical AGN continuum, there is a surface layer of thickness $N_H \sim 10^{23} U$ cm^{-2}, where H is mostly ionized. At the surface of this "H II" layer there is a thinner "He III" layer. For a typical AGN continuum the column density of the "He III" layer is N_H(He III) $\sim 2 \times 10^{21} U$ cm^{-2}. Thus, irrespective of the value of U, the "He III" layer is about 3 times thicker than the upper limit of $N_H \leq 6 \times 10^{20} U$ cm^{-2} deduced from the UV absorber in I Zw 1. The He in the UV absorber would be mostly He III, and the soft X-ray absorption would originate in the residual He II within the UV absorber. The He III/He II fraction within the "He III" region is given by $N_{He\,III}/N_{He\,II} \simeq 10^3 U$ (Netzer 1990). The upper limit on the He II column density in the UV absorber is then

$$N_{He\,II} = N_H \times \frac{N_{He}}{N_H} \times \frac{N_{He\,II}}{N_{He}} \leq 6 \times 10^{20} U \times 0.1 \times (10^3 U)^{-1} ,$$

i.e., $N_{He\,II} = 6 \times 10^{16}$ cm^{-2}, which is $\sim$300 smaller than the $N_{He\,II}$ required to produce the X-ray absorption. It thus appear that the upper limit on the column of the layer that produces the UV absorption is much smaller than that required to produce the possible X-ray absorption.

This line of argument suggests that the UV and X-ray absorbers are distinct. However, given the uncertainty in the upper limit on the Lyα absorption EW, which sets N_H, and the uncertainty in the far UV spectral shape, which sets $N_{He\,III}(U)$, we cannot conclusively rule out the possibility that an "He II" region is present behind the "He III" region. Such an "He II" region can produce a high He II column, which would be required if the X-ray absorption is real, together with a relatively small total H I column, implied by the UV absorption lines.

4.3. *UV and Optical Emission*

The UV absorber blueshift of $\sim$1870 km s^{-1} is remarkably close to the He II λ1640 emission-line blueshift of $\sim$1990 km s^{-1}, suggesting that the strongly blueshifted He II emission-line peak may originate in the same outflowing gas that produces the UV absorption lines. In order to emit the observed He II λ1640 flux, the absorber must absorb most photons just above the He II bound-free edge at 4 Ryd. As described above, when $N_H \sim 6 \times 10^{20} U$ cm^{-2}, the UV absorber is within a factor of 3 of the column density required to form an "He II" region; i.e., it absorbs $\sim\frac{1}{3}$ of He II ionizing photons, and thus if the column density of the UV absorber is close to the upper limit, and its covering factor is close to unity, it may contribute significantly to the observed He II λ1640 emission.

The intrinsic X-ray absorber becomes optically thick below 0.2 keV. It is therefore highly optically thick at 4 Ryd and can produce the observed He II λ1640 emission if its covering factor is reasonably large ($>10\%$).

It is interesting to note that Oke & Lauer (1979) found evidence for [O III] λ5007 and [Ne III] λ3868 emission components at $z = 0.0548$, which corresponds to a $\sim$1800 km s^{-1} blueshift with respect to the $z = 0.0608$ used here. The same feature was also noted by van Groningen (1993) in a high spectral resolution profile of [O III] λ5007. If these emission components also originate in the UV absorber, then their flux can be used as an additional constraint on the density, column density, and ionization parameter of the UV absorber.

4.4. *Future Observations*

Higher spectral resolution observations of the Lyα, N V, and C IV absorption lines would allow a much more accurate determination of the absorption profile, and thus of the absorber's column. If the H I column density is indeed close to the upper limit, as required to "unite" the UV absorption, X-ray absorption, and He II emission, then the Lyα absorption profile, for example, would appear as a $\sim$60 km s^{-1} wide, steep-sided, and flat-bottomed trough going down to zero flux. The metal absorption lines should also be resolved as deep, narrow, optically thick absorption lines with damping wings. If the absorption lines remain shallow

and broad, then the lower limits to the absorbing columns would apply. The metal lines absorption doublet ratios can be used to establish the covering factor of the UV absorber.

Higher S/N X-ray spectra below 0.5 keV are required to establish whether the soft X-ray absorption hinted at by the *ROSAT* PSPC is indeed real.

5. DISCUSSION

The strong optical Fe II emission of I Zw 1, its weak [O III] emission, strong IR emission, and "red" UV continuum are all typical properties of low-ionization broad absorption line quasars (BALQSOs; Weymann et al. 1991; Boroson & Meyers 1992; Sprayberry & Foltz 1992). The presence of weak UV absorption at a blueshift of ~ 2000 km s^{-1} in I Zw 1 suggests it may be a "failed" low-ionization BALQSO, i.e., a BALQSO where our line of sight just grazes the outflowing high-ionization wind and misses the low-ionization outflow, as suggested by Turnshek et al. (1994) in the case of PG 0043+039.

Are the red continuum, excess blue flux in the high-ionization lines, associated absorption, and dense BLR, unique to I Zw 1, or are they typical UV properties of narrow-line quasars? No complete UV study of narrow-line AGNs is available to answer these questions, but some hints may be obtained from existing observations (see also discussion in Lawrence et al. 1997).

Baldwin et al. (1996) studied the emission-line properties of a heterogeneous sample of seven $z \sim 2$ quasars with a range of emission-line properties. Some of their objects have strong Fe II, Fe III, and Al III emission as observed in I Zw 1. Baldwin et al. analyzed in detail the UV spectrum of Q0207−398, where a high S/N was available, and found excess emission in the blue wing of the high-ionization UV lines, which they interpreted as a high-ionization outflowing component in the BLR, although there was no direct evidence (through absorption) for such a component, as probably observed in I Zw 1.

It is also interesting to note that BG92 found that strong optical Fe II emitting quasars, which tend to have narrow Hβ, also tend to have blue excess flux in Hβ, and Boroson & Meyers found that low-ionization BALQSOs, which are generally I Zw 1–like, have blue excess flux in Hα. It is not known, however, whether this property extends to the UV lines as well.

If the UV absorption system in I Zw 1 is indeed producing the blueshifted components of the high-ionization lines, then the absence of a corresponding redshifted component indicates that the far side of this outflow has to be obscured. This may either be due to an extended highly optically thick gas, such as an accretion disk, or it may result from absorption within each cloud, if the clouds column density is large enough (see Ferland et al. 1992 for discussion).

The doublet ratios observed here indicate that the low-ionization lines are thermalized and will not be emitted isotropically. However, the large velocity gradients in the wind may strongly reduce the optical depth for the high-ionization lines in the wind. The observed blueshifted emission in C IV and N V is far too broad to determine the observed doublet ratio and cannot be used to determine if the emission from that gas is optically thick or thin.

I Zw 1 has particularly weak C III] λ1909 emission (§ 3.1.2) but normal Si III] λ1892 emission, which we interpret here as evidence for a relatively dense ($\sim 10^{11}$ cm^{-3}) BLR, at least for the region that produces the low-ionization lines. Baldwin et al. (1988) noted the weakness of C III] λ1909 in four other quasars with narrow UV lines, and this trend is also apparent in Baldwin et al. (1996) quasars. The most extreme case is of H0335−336, where essentially no C III] λ1909 emission was observed (Hartig & Baldwin 1986). This quasar has very narrow lines, and is also a low-ionization BALQSO.

Independent evidence for a dense BLR with $n_e \gtrsim 10^{11}$ cm^{-3} is provided by the significant EW and thermalized doublet ratio of the Al III λ1857 doublet (§ 3.1.6) and by the significant EW of C III* λ1176 (§ 3.1.2). Another indication for a dense BLR in I Zw 1 is provided by its optical spectrum. The Na I $\lambda\lambda$5889.95, 5895.92 emission line is rather strong (Oke & Lauer 1979; Phillips 1976), which Thompson (1991) and Korista et al. (1997, their Fig. 3*g*) find can be produced only for $n_e \gtrsim 10^{11}$ cm^{-3}, and a large column density (required to shield neutral Na I from ionizing radiation at $E > 5.14$ eV).

I Zw 1 has a "red" continuum (§ 3.3), which is rather rare among quasars. Two of the four quasars with narrow lines described by Baldwin et al. (1988) also have a $\alpha \approx -1$ UV spectral slope, but the other two narrow-line quasars have $\alpha \approx 0$ and -0.5, which are typical values.

It thus appears that some of the properties of I Zw 1, in particular the relatively weak C III] λ1909, and the blueshifted excess emission in the high-ionization lines, may be common in narrow-line quasars. A more systematic study of the UV emission of narrow-line AGNs is required to establish their typical emission-line properties, their relation to low-ionization BALQSOs, and to eventually understand the underlying physics.

6. SUMMARY

A high S/N UV spectrum of I Zw 1 was obtained with the *HST* FOS with a spectral resolution of $\lambda/\Delta\lambda \sim 1300$ over the 1150–3250 Å spectral region. The following main results are obtained from our analysis of the UV spectrum of I Zw 1.

1. The Mg II λ2798 doublet is partially resolved. The measured doublet ratio is 1.2/1, consistent with theoretical predictions that the BLR is highly optically thick to absorption in this line.

2. The Al III λ1857 doublet is clearly resolved with an "optically thick" doublet ratio of 1.25/1. The line optical depth provides an upper limit to the clouds distance from the ionizing source that is consistent with the "standard" BLR radius. The strength of this line requires a BLR component with $n_e \gtrsim 4 \times 10^{11}$–$4 \times 10^{12}$ cm^{-3}.

3. A weak UV absorption system is detected in N V, and possibly C IV and Lyα as well, indicating an outflow with a line-of-sight velocity of ~ 1870 km s^{-1} and velocity dispersion $\lesssim 300$ km s^{-1}.

4. Lines from ions of increasing ionization level show increasing excess flux on the blue wing and an increasing shift in the velocity of the emission-line peak, reaching a maximum blueshift of ~ 2000 km s^{-1} for He II λ1640. This may indicate an outflowing component in the BLR, visible only in the approaching direction, where the ionization level increases with velocity. The highest velocity part of this outflow may produce the observed UV absorption system.

5. The small C III] λ1909 EW and the small C III] λ1909/Lyα and C III] λ1909/Si III]λ1892 flux ratios indicate that

the bulk of the gas in the BLR has a density of 10^{11} cm^{-3}, about an order of magnitude larger than typically seen in AGNs.

6. Very weak [C III] λ1907 and [Si III] λ1883 emission may be present, indicating there may be an NLR component with $n_e \sim 5 \times 10^5$ cm^{-3}.

7. The C III* λ1176 line is clearly detected. Its strength indicates a BLR component with $n_e \gtrsim 10^{11}$ cm^{-3}.

8. Prominent Fe II UV 191 emission is seen, together with weaker emission lines at 1294 Å and 1871 Å. These three features have been proposed in the literature as evidence for significant Lyα pumping of the 8–10 eV levels of Fe II.

9. Significant Fe III emission is present. Fe III UV 34 and UV 48 multiplets are clearly resolved, and Fe III UV 1, UV 47, UV 50, and UV 68 may also be present. The implications of significant Fe III emission for the conditions in the BLR needs to be explored.

10. The suggestion by Grandi (1983) that the O I λ1304 emission line is partly converted to O I] λ1641 is ruled out in the case of I Zw 1, indicating that the bulk of O I Lyβ Bowen fluorescence occurs in the BLR clouds at a depth where $\tau_{\mathrm{Ly}\alpha} < 10^9$. The strong suppression of O I λ1304 in I Zw 1 is due either to reddening or to Balmer continuum absorption.

The *HST* spectrum of I Zw 1 demonstrates the richness and complexity of quasars' emission-line spectra. It is not clear whether some of the emission features are unique to I Zw 1 or whether they are typical of most AGNs. Many of the features detected here would be blended and unidentifiable in typical quasar spectra, creating a deceptively simple emission spectrum. A close inspection of the Francis et al. composite (Fig. 1) suggests that most of the features detected here are indeed present in other AGNs. The rich UV emission spectrum of I Zw 1 should serve as a useful benchmark for photoionization codes, in particular, for codes attempting to calculate the complex emission spectrum of Fe II. Many weak features remain unidentified, and it is likely that at least some of these are weak Fe II features. A reliable identification of these weak features may follow from detailed photoionization models. The high-quality optical-UV spectrum of I Zw 1 obtained in this study can be used for constructing an Fe II UV template and is available on request from the authors.

Support for this work is provided in part by NASA through grant GO-5486.01-93A from the Space Telescope Science Institute and by a grant to A. L. from the Israel Science Foundation. We thank C. L. Joseph for his help in obtaining the ground-based spectrum of I Zw 1 and the referee for a careful reading of the paper and helpful comments.

REFERENCES

Baldwin, J. A., McMahon, R., Hazard, C., & Williams, R. E. 1988, ApJ, 327, 103
Baldwin, J. A., & Netzer, H. 1978, ApJ, 226, 1
Baldwin, J. A., et al. 1996, ApJ, 461, 664
Bergeron, J., & Kunth, D. 1984, MNRAS, 207, 263
Boller, T., Brandt, W. N., & Fink, H. 1996, A&A, 305, 53
Boroson, T. A., & Green, R. F. 1992, ApJS, 80, 109 (BG92)
Boroson, T. A., & Meyers, K. A. 1992, ApJ, 397, 442
Bromage, G. E., et al. 1985, MNRAS, 215, 1
Collin-Souffrin, S., & Dumont, S. 1986, A&A, 166, 13
Corbin, M. R. 1990, ApJ, 357, 346
Diplas, A., & Savage, B. D. 1994, ApJ, 427, 273
Dufton, P. L., & Kingston, A. E. 1987, J. Phys. B., 20, 3899
Elvis, M., Lockman, F. J., & Wilkes, B. J. 1989, AJ, 97, 777
Espey, B. R., Carswell, R. F., Bailey, J. A., Smith, M. G., & Ward, M. J. 1989, ApJ, 342, 666
Ferguson, J. W., Ferland, G. J., & Pradhan, A. K. 1995, ApJ, 438, L55
Ferland, G. J., Peterson, B. M., Horne, K., Welsh, W. F., & Nahar, S. N. 1992, ApJ, 387, 95
Francis, P. J., Hewett, P. C., Foltz, C. B., Chaffee, F. H., Weymann, R. J., & Morris, S. 1991, ApJ, 373, 465
Gaskell, C. M. 1982, ApJ, 263, 79
Grandi, S. A. 1983, ApJ, 268, 591
Hamann, F. 1997, ApJS, 109, 279
Hamann, F., Shields, J. C., Cohen, R. D., Junkarinen, V. T., & Burbidge, E. M. 1997, in IAU Coll. 159, Emission Lines in Active Galaxies: New Methods and Techniques, ed. B. M. Peterson, F. Z. Cheng, & A. S. Wilson (ASP Conf. Ser. 113; San Francisco: ASP), 96
Hamann, F., Shields, J. C., Ferland, G. J., & Korista, K. T. 1995, ApJ, 454, 688
Hartig, G. F., & Baldwin, J. A. 1986, ApJ, 302, 64
Johansson, S., & Hamann, F. W. 1993, Phys. Scr., T47, 157
Johansson, S., & Jordan, C. 1984, MNRAS, 210, 239
Joly, M. 1981, A&A, 102, 321
Kaspi, S., Smith, P. S., Maoz, D., Netzer, H., & Jannuzi, B. T. 1996, ApJ, 471, L75
Keenan, F. P., Feibelman, W. A., & Berrington, K. A. 1992, ApJ, 389, 443
Korista, K., Baldwin, J., Ferland, G., & Verner, D. 1997, ApJS, 108, 401
Kriss, G. A., et al. 1996a, ApJ, 467, 629
Kriss, G. A., Espey, B. R., Krolik, J. H., Tsvetanov, Z., Zheng, W., & Davidsen, A. F. 1996b, ApJ, 467, 622
Kwan, J. 1984, ApJ, 283, 70
Kwan, J., & Krolik, J. H. 1981, ApJ, 250, 478
Laor, A., Bahcall, J. N., Jannuzi, B. T., Schneider, D. P., & Green, R. F. 1995, ApJS, 99, 1
Laor, A., Bahcall, J. N., Jannuzi, B. T., Schneider, D. P., Green, R. F., & Hartig, G. F. 1994a, ApJ, 420, 110
Laor, A., & Draine, B. T. 1993, ApJ, 402, 441
Laor, A., Fiore, F., Elvis, M., Wilkes, B. J., & McDowell, J. C. 1994b, ApJ, 435, 611
———. 1997a, ApJ, 477, 93
Laor, A., Jannuzi, B. T., Green, R. F., & Boroson, T. A. 1997b, in IAU Coll. 159, Emission Lines in Active Galaxies: New Methods and Techniques, ed. B. M. Peterson, F. Z. Cheng, & A. S. Wilson (ASP Conf. Ser. 113; San Francisco: ASP), 116
Lawrence, A., Elvis, M., Wilkes, B. J., McHardy, I., & Brandt, N. 1997, MNRAS, 285, 879
Lipari, S. 1994, ApJ, 436, 102
Lipari, S., Terlevich, R., & Macchetto, F. 1993, ApJ, 406, 451
Maoz, D. 1995, in Reverberation Mapping of the BLR of AGN, ed. P. M. Gondhalekar, K. Horne, & B. M. Peterson (San Francisco: ASP), 95
Mathur, S., Elvis, M., & Wilkes, B. 1995, ApJ, 452, 230
Mathur, S., Wilkes, B., Elvis, M., & Fiore, F. 1994, ApJ, 434, 493
Miley, G. K., & Miller, J. S. 1979, ApJ, 228, L55
Moore, C. E. 1952, An Ultraviolet Multiplet Table (NBS Circular 488; Washington: U.S. Dept. Commerce)
———. 1959, A Multiplet Table of Astrophysical Interest (rev. ed.; NBS Technical Note 36; Washington: U.S. Dept. Commerce)
Morton, D. C. 1991, ApJS, 77, 119
Netzer, H. 1990, in Active Galactic Nuclei, ed. T. J. L. Courvoisier & M. Mayor (Berlin: Springer), 57
Netzer, H., Brotherton, M. S., Wills, B. J., Han, M., Wills, D., Baldwin, J. A., Ferland, G. J., & Browne, I. W. A. 1995, ApJ, 448, 27
Netzer, H., Elitzur, M., & Ferland, G. J. 1985, ApJ, 299, 752
Netzer, H., & Laor, A. 1993, ApJ, 404, L51
Netzer, H., & Wills, B. J. 1983, ApJ, 275, 445
Neugebauer, G., Green, R. F., Mathews, K., Schmidt, M., Soifer, B. T., & Bennet, J. 1987, ApJS, 63, 615
Oke, J. B., & Lauer, T. R. 1979, ApJ, 230, 360
Osterbrock, D. E. 1989, Astrophysics of Gaseous Nebulae and Active Galactic Nuclei (California: Univ. Sci. Books)
Penston, M. V. 1987, MNRAS, 229, 1p
Peterson, B. 1993, PASP, 105, 247
Phillips, M. M. 1976, ApJ, 208, 37
———. 1977, ApJ, 215, 746
———. 1978, ApJS, 38, 187
Pradhan, A. K., & Peng, J. 1995, in The Analysis of Emission Lines, ed. R. E. Williams & M. Livio (Cambridge: Cambridge Univ. Press), 8
Rudy, R. J., Rossano, G. S., & Puetter, R. C. 1989, ApJ, 342, 235
Sargent, W. L. W. 1968, ApJ, 152, L31
Savage, B. D., et al. 1993, ApJ, 413, 116
Schneider, D. P., et al. 1993, ApJS, 87, 45
Seaton, M. J. 1979, MNRAS, 187, 73p
Smith, P. S., Schmidt, G. D., Allen, R. G., & Hines, D. C. 1997, ApJ, in press
Sprayberry, D., & Foltz, C. B. 1992, ApJ, 390, 39

Storey, P. J. 1981, MNRAS, 195, 27p
Thompson, K. L. 1991, ApJ, 374, 496
Turnshek, D. A., et al. 1994, ApJ, 428, 93
Tytler, D., & Fan, X. M. 1992, ApJS, 79, 1
Uomoto, A. 1984, ApJ, 284, 497
van Groningen, E. 1993, A&A, 272, 25
Verner, D. A., & Yakovlev, D. G. 1995, A&AS, 109, 125
Véron-Cetty, M. P., Véron, P. 1991, A Catalogue of Quasars and Active Nuclei (5th ed.; Munich: ESO)
Weymann R. J., Morris, S. L., Foltz, C. B., & Hewett, P. C. 1991, ApJ, 373, 23
Wilkes, B. J. 1984, MNRAS, 207, 73
———. 1986, MNRAS, 218, 331
Wills, B. J. 1983, in Proc. 24th Liege International Astrophysical Colloquium, Quasars and Gravitational Lenses, ed. J. P. Swings (Liege: Universite de Liege, Institut d'Astrophysique), 458
Wills, B. J., Brotherton, M. S., Fang, D., Steidel, C. C., & Sargent, W. L. W. 1993, ApJ, 415, 563
Wills, B. J., Netzer, H., & Wills, D. 1980, ApJ, 242, L1
———. 1985, ApJ, 288, 94
Wills, B. J., et al. 1995, ApJ, 447, 139
Wills, D., & Netzer, H. 1979, ApJ, 233, 1